Initial clinical experience using ^{68}Ga-FAPI-46 PET/CT for detecting various cancer types

Habibollah Dadgar[1] MSc, Nasim Norouzbeigi[1] MD, Majid Assadi[2] MD, Batool Al-balooshi[3] MD, Akram Al-Ibraheem[4,5] MD, Abdulredha A. Esmail[6] MD, Fahad Marafi[7] MD, Mohamad Haidar[8] MD, Haider Muhsin Al-Alawi[9,10] MD, Yehia Omar[11] MD, Sharjeel Usmani[12] MD, Andrea Cimini[13] MD, Hossein Arabi[14] PHD, Habib Zaidi[14,15,16,17†] PhD

1. Cancer Research Center, RAZAVI Hospital, Imam Reza International University, Mashhad, Iran
2. The Persian Gulf Nuclear Medicine Research Center, Department of Molecular Imaging and Radionuclide Therapy (MIRT), Bushehr Medical University Hospital, Bushehr University of Medical Sciences, Bushehr, Iran
3. Dubai Nuclear medicine & Molecular imaging Center-Dubai, Hospital-Dubai Health-DH, UAE
4. Department of Nuclear Medicine, King Hussein Cancer Center, Amman, Jordan
5. Division of Nuclear Medicine/Department of Radiology and Nuclear Medicine, University of Jordan, Amman, Jordan
6.Nuclear Medicine Department, Kuwait Cancer Control Center, Kuwait City, Kuwait
7. Jaber Alahmad Center of Nuclear Medicine and Molecular Imaging, Kuwait City, Kuwait
8. Diagnostic Clinical Radiology Department, Division of Nuclear Medicine, American University of Beirut, Beirut, Lebanon
9. Nuclear Medicine department, Amir Al-momineen Specialty Hospital, Al-Najaf Governorate, Iraq
10. Middle Euphrates Cancer Hospital, Al-Najaf Governorate, Iraq
11. PET/CT department at Misr Radiology Center, Heliopolis, Egypt
12. Department of Nuclear Medicine Sultan Qaboos Comprehensive Cancer Care and Research Center (SQCCCRC) ,Seeb, Oman,
13. Nuclear Medicine Unit, St. Salvatore Hospital, 67100 L'Aquila, Italy
14. Division of Nuclear Medicine and Molecular Imaging, Department of Medical Imaging, Geneva University Hospital, CH-1211 Geneva, Switzerland
15. Department of Nuclear Medicine and Molecular Imaging, University of Groningen, University Medical Center Groningen, 9700RB Groningen, Netherlands
16. Department of Nuclear Medicine, University of Southern Denmark, Odense, Denmark,
17. University Research and Innovation Center, Óbuda University, Budapest, Hungary

Keywords: PET/CT - ^{68}Ga-FAPI - ^{68}Ga-DOTATATE - ^{68}Ga-Pentixafor - ^{18}F-FDG

Corresponding author:
Habib Zaidi PhD,
Geneva University Hospital
Division of Nuclear Medicine and Molecular Imaging CH-1211 Geneva, Switzerland
Tel:+41223727258
Fax: +4122 3727169
habib.zaidi@hcuge.ch

Received:
23 April 2024
Accepted revised:
24 June 2024

Abstract

Objective: Numerous studies have shown that gallium-68-labeled fibroblast activation protein inhibitor (^{68}Ga-FAPI) positron emission tomography/computed tomography (PET/CT) scans would yield high intra-tumoral tracer uptake and low uptake in normal tissues as background, thus allowing for excellent visualization of lesions in the cancer micro environment. This study set out to compare the suit ability of novel ^{68}Ga-FAPI-46 PET versus routine fluorine-18-fluorodeoxyglucose (^{18}F-FDG) PET and other few cases of ^{68}Ga-DOTATATE/^{68}Ga-Pentixa for PET/CT for the assessment of different types of cancer. **Subjects and Methods:** A retrospective analysis of 11 patients (6 males, 5 females; average age: 53 years, range: 10-58 years) with histopathologically confirmed, well-differentiated adenocarcinoma, medullar thyroid cancer (MTC), papillary thyroid carcinoma (PTC), cervical, gastric, glioblastoma multiform (GBM), colon, Ewing's sarcoma, and breast cancer was performed. These patients underwent PET/CT scans using four different radio-tracers (9 ^{18}F-FDG,11 ^{68}Ga-FAPI, 3 ^{68}Ga-DOTATATE, and 1 ^{68}Ga-Pentixafor). The patients' PET/CT images were visually evaluated for cancer detection, and analyzed semi-quantitatively through image-derived metrics, such as target-to-background ratio (TBR) and maximum standardized uptake value (SUVmax), for recurrence and metastasis. **Results:** The study of 11 patients revealed that ^{68}Ga-FAPI-46 was more effective than other tracers for detecting metastases, with 55 vs. 49 metastases in the lymph nodes, 4 vs. 3 in the liver, and 4 vs. 3 in the bones detected in comparison to ^{18}F-FDG. No significant differences were observed in ^{68}Ga-DOTATATE and ^{68}Ga-Pentixafor PET images. In addition, in five patients, the SUVmax and TBR values in ^{68}Ga-FAPI-46 PET images were significantly higher than those in ^{18}F-FDG PET images for lymph nodes and bone metastases. Although the SUVmax in ^{68}Ga-FAPI-46 and ^{18}F-FDG PET images for liver metastases was comparable, ^{68}Ga-FAPI-46 had a significantly higher TBR than ^{18}F-FDG. **Conclusions:** Our findings suggest that FAPI PET/CT is not suitable for evaluating GBM and Ewing sarcoma but generally outperforms ^{18}F-FDG PET/CT in various types of breast cancer, gastrointestinal, gynecological, PTC and MTC. However, larger trials are needed to validate these preliminary findings.

Hell J Nucl Med 2024; 27(2): 105-120 *Epub ahead of print: 6 August 2024* *Published online: 28 August 2024*

Introduction

Recently, the tumor microenvironment (TME) has emerged as a therapeutic target in cancer treatment and imaging [1]. Cancer-associated fibroblasts (CAF) area constitutive part of TME and are abundant in the stroma of tumors, such as colon and breast cancer [2]. Fibroblast activation protein (FAP), characteristic of cancer-associated fibroblasts, is a type II membrane-bound serine protease that is part of the dipeptidyl peptidase group [3]. The differential FAP expression in normal tissues versus inflammation/ tumors renders FAP a promising target for nuclear/molecular imaging of tumors and some non-oncological diseases. Over 90% of epithelial tumors, including breast, colon, lung, ovarian, and pancreatic adenocarcinomas, show elevated expression of FAP on their CAF. Though the prognostic value of FAP in different cancer types has been contradictory in the literature, high FAP expression indicates poor prognostic outcomes (could be regarded as an independent marker), particularly in hepatocellular carcinoma, colon, and lung cancer [4-6]. In this light, FAP-targeted radiopharmaceuticals based on FAP-specific inhibitors (FAPI), such as gallium- 68 (^{68}Ga)-FAPI-02 and ^{68}Ga-FAPI-04 have been recently developed [7, 8]. High intra-tumoral uptake and rapidrenal clearance of these tracers, combined with relatively very low uptake/concentration in normal organs, would result in a higher tumor-to-background ratio (TBR) and improved PET imaging diagnostic performance [7, 9, 10]. Furthermore, the use of DOTA or other chelating agents allows for the easy incorporation of therapeutic isotopes, such as lutetium-177 (^{177}Lu), yttrium-90 (^{90}Y),

and actinium-225 (^{225}Ac) into these compounds, thus enabling theranostic treatments [8]. However, FAPI tracers' relatively short tumor retention times continue to limit their therapeutic potential. Fifty percent tumor uptake within 1 to 3 hours post-injection indicates that FAPI-04 is superior to FAPI-02 (75 % washout) in terms of tumor retention. Fibroblast activation protein inhibitor-46, a newly developed radiotracer with alonger tumor residence time [11], enables theranostic treatments. Fibroblast activation protein inhibitor-46 was chosen from 15 other FAPI variants, owing to its superior pharmacokinetics and tumor-to-background ratio (TBR). Fibroblast activation protein inhibitor radiopharmaceuticals have shown high urinary uptake and concentration, with the kidneys serving as the primary excretory organ. The relatively high uptake of FAPI radiopharmaceuticals was also observed in the bile duct and gallbladder, which indicates radiotracer washout/removal via the hepatobiliary system. Other organs such as the submaxillary gland, thyroid, and pancreas exhibited a moderate absorption of the radiotracer. In contrast, various organs/tissues like the brain, parotid gland, buccal mucosa, lung, myocardium, liver, intestine, fat, spine, and muscle showed minimal to low radio-tracer uptake [7, 9]. So far, drug-related pharmacological effects or physiological responses of FAP inhibitors have not been seen in clinical investigations, implying the application of these radiotracers for positron emission tomography (PET) imaging [7, 9]. Positron emission tomography/computed tomography (CT) imaging using ^{68}Ga-FAPI-46 at an initial time frame (10 minutes after injection) showed a similar rate of lesion identification as that of a later time frame (60 minutes post-injection) [12]. Recent research [10, 13-19] suggests that ^{68}Ga-FAPI-46 could replace ^{18}F-FDG PET/CT as a more accurate and practical option for the diagnosis and staging of various cancers, especially metastases to the lymph nodes, brain, and bones. In this study, we present our preliminary findings from PET imaging with ^{68}Ga-FAPI-46 in patients with metastatic cancer at an advanced stage.

Gallium-68-DOTATOC, ^{68}Ga-DOTATATE, and ^{68}Ga-DOTANOC are radiotracers for somatostatin receptors (SSTR) PET/CT imaging (^{68}Ga-DOTA conjugated peptides), considered the current gold standard for imaging of neuroendocrine tumors (NET) [20]. The enhanced performance of SSTR-PET/CT imaging in comparison to scintigraphy and traditional diagnostic techniques is well-documented, especially in the identification of small lesions, lymph nodes, and bone metastases. A recent comprehensive review summarized results from 34 meta-analyses, evaluating the diagnostic efficacy of various radiopharmaceuticals (such as SSTR, DOPA, and ^{18}F-FDG PET/CT) in NET PET imaging and its clinical ramifications [21]. Somatostatin receptors PET/CT demonstrated outstanding sensitivity and specificity in well-differentiated NET expressing SSTR (90%) and impacted the clinical approach in ne-arly 40% of instances. Present-day recommendations advo-cate for the use of ^{68}Ga-DOTA-linked peptide PET/ CT for the purposes of staging, reevaluation post-treatment, and prognostic assessment [20, 22]. Additionally, employing PET/CT with ^{68}Ga-DOTA-bound peptides is crucial for in vivo confirmation of SSTR expression and pinpointing patients who could potentially benefit from peptide receptor radionuclide therapy (PRRT).

Gallium-68-pentixafor and its therapeutic counterpart,^{177}Lu-pentixather, have been introduced as potential new agents for imaging brain tumors and delivering targeted radionuclide treatment. Gallium-68-pentixafor targets the C-X-C chemokine receptor type 4 (CXCR4), a G protein-linked receptor for the stromal-derived factor 1 (SDF-1) ligand, which is also referred to as C-X-C motif chemokine 12 (CXCL12). This interaction inhibits the macrophage inhibitory factor (MIF). Among glioblastoma patients, this association correlates with a negative prognosis and a more invasive phenotype [23-25]. Indeed, CXCR4 plays a pivotal role in controlling the tumor microenvironment and the spread of metastases. Additionally, CXCR4 can be tagged with beta-emitting cytotoxins like ^{177}Lu or ^{90}Y. This has given rise to the innovative theranostic agent, Pentixather, designed for CXCR4-focused endoradiotherapy. It has been trialed with mixed outcomes in conditions like multiple myeloma and various hematological malignancies [26, 27]. Given that this treatment leads to bone marrow suppression, further research is necessary to evaluate its efficacy in cancer management.

Subjects and Methods

Patient population

The RAZAVI Hospital Ethics Committee approved this study protocol, which was conducted from July 2021 to September 2022. All participants provided their consent through a signed written form. The criteria for inclusion in this study were: (i) subjects with a minimum age of 10 years; (ii) subjects who underwent ^{68}Ga-FAPI-46 and either ^{18}F-FDG/^{68}Ga-Pentixafor, or ^{68}Ga-DOTATATE PET/CT atone-week intervals without receiving therapeutic options through the imaging time points; (iii) patients scheduled for PET/CT with indications for initial staging or suspected recurrence. The patient population consisting of 11 patients underwent a ^{68}Ga-FAPI-46 PET scan. Among these patients, 9, 3, and 1 also underwent ^{18}F-FDG, ^{68}Ga-DOTATATE, and ^{68}Ga-Pentixafor PET scans. One patient underwent 3 PET scans with three radiotracers including ^{68}Ga-FAPI-46/^{68}Ga-DOTATATE/^{68}Ga-Pentixafor PET/CT imaging.

PET/CT imaging

Participants were asked to fast at least 6 hours and avoid heavy activity or prolonged exercise prior to intravenous injection of ^{18}F-FDG (3.7MBq/kg). Patients were also required to have normal blood glucose levels. No special fasting or glycemic preparation was required for ^{68}Ga- FAPI-46, ^{68}Ga-Pentixafor, and ^{68}Ga-DOTATATE, where PET/CT acquisition was conducted after intravenous injection of 1.85-2.59MBq/kg activity. A hybrid Biograph 6 PET/CT scanner (Siemens Healthcare, Erlangen, Germany) was used to perform all PET/CT imaging approximately one hour after injection. Patients were asked to raise their arms overhead, and an initial spiral CT scan was performed from the skullcap to the upper part of the mid-thigh using the following acquisition parameters: 120mA tube current; 120kV tube voltage; 512×512 pixels

matrix; 3mm slice thickness; 300-500HU window width. Positron emission tomography acquisition was performed with 2.2min/bed position in 3D acquisition mode using an overall 5-6 bed positions. Computed tomography based PET attenuation correction was carried out on the PET data and the reconstruction was performed using an ordered subset maximization algorithm with 21 subsets and 2 iterations.

Clinical imaging review

A pair of experienced nuclear medicine experts independently conducted both a visual evaluation and a semi-quantitative analysis of all PET/CT images. Lesions with active tracer absorption were pinpointed by regions show casing non-typical uptake surpassing the background across all scans. These identified lesions were subsequently classified either as non-malignant, distant metastatic, or lymphatic metastatic. Positron emission tomography images of two radiotracers (^{68}Ga-FAPI-46 vs. ^{18}F-FDG, ^{68}Ga-FAPI-46 vs. ^{68}Ga-DOTATATE, and ^{68}Ga-FAPI-46 vs ^{68}Ga-Pentixafor) were first compared via a visual assessment where in the two images were rated for each patient in terms of the number of identified lesions. Semi-quantitative analysis was then performed by comparing the uptake of the radiotracer within the same lesions. The maximum standardized uptake value (SUVmax) was measured for regions of interest (ROI) defined on the lesion by a physician. The tumor-to-background ratio (TBR), defined as the ratio of lesion SUVmax to background SUVmean (Eq. 1), was calculated for the malignant lesions and the different radiotracers.

$$TBR = \frac{Lesion\ SUV_{max}}{Background\ \ SUV_{mean}} \quad (1)$$

Statistical analysis

The data was analyzed using the SPSS software (v. 26.0; IBM, NY, USA). Outcomes from the various radiotracers underwent a descriptive examination. Categorical variables were represented as counts and percentages, while continuous variables were displayed as means with standard deviations. The Chi-square test was utilized to contrast the count of positive lesions. To compare the SUVmax and TBR metrics of lesions in the distinct PET/CT scans, we employed Student's t-tests.

Results

The characteristics of the registered cases are shown in Table 1. Clinical diagnosis was confirmed through histopathology for well-differentiated adenocarcinoma (ADC), medullary thyroid cancer (MTC), papillary thyroid cancer (PTC), cervical, gastric, glioblastoma multiform (GBM), colon, Ewing's sarcoma, and breast cancer who underwent ^{68}Ga-FAPI-46 and ^{18}F-FDG PET/CT scans. The mean tumor size was 2.6± 1.7cm, with a minimum and maximum length of 1.2cm and 5.4cm, respectively. Overall, 9 patients underwent surgical resection, 3 patients received a concurrent cycle of ^{177}Lu-DOTATATE and ^{177}Lu-Trastozumab. In addition, 7 patients received chemotherapy cycles at least eight months before dual-tracer imaging. The remaining two patients underwent non-surgical anti-tumor treatment.

Comparison of visual assessment

After assessment of ^{68}Ga-FAPI-46 PET and ^{18}F-FDG scans 49

Table 1. *Characteristics of patients involved in this study.*

No.	Sex	Age	Pathology	Metastases sites	Indication
1	M	46	Well differentiated ADC	5 liver mass lesions in both liver lobes	Response
2	F	46	PTC	Possibility of initial phases of heterotopic ossification lateral to the resected region of right sacroiliac bone, cannot be ruled out	Metastatic
3	F	58	Cervix cancer	Peritoneum and mass lesion in the left side of the pelvic more compatible with peritoneal seeding and mesenteric involvement.	Recurrence
4	M	58	Gastric ADC	Hypermetabolic cervical lymph node (LN) in the right side of the neck (level 2) without FAPI uptake. For definite diagnosis tissue sampling is recommended.	Recurrence
5	M	55	GBM	Right frontotemporal lobes	Metastatic
6	M	53	Gastric ADC	Cardia region	Recurrence
7	F	41	Colon ADC	Peritoneal seeding and mesenteric LNs metastasis	Metastatic
8	M	10	Ewing sarcoma	Left fibula	Recurrence
9	F	53	Breast cancer	Left breast, left axillary LNs	Metastatic
10	M	33	MTC	Right upper paratracheal	Metastatic
11	F	31	MTC	LNs in the superior mediastinum, paratracheal and pre-carinal	Metastatic

and 55 involved lymph nodes were identified, respectively. Overall, there were 31 sites (1 brain, 3 neck, 5 supraclavicular, 4 axilla, 7 mediastinum, 3 bone, 4 liver, and 4 intra-abdomen) of nodal involvement in 12 patients detected by both tracers. Fluorine-18-FDG PET/CT detected more lymph nodes than ^{68}Ga-FAPI-46 PET/CT; however, the numbers of involved sites were not different between the two tracers. The sizes of the detected nodes ranged from 0.3cm to 3.1cm. Figure 1 depicts a patient who had the lowest nodal detection by ^{68}Ga-FAPI-46 tracer.

Moreover, higher uptake was observed in the uterus in the right lower image in the MIP of the ^{68}Ga-FAPI-46 PET/CT scan (physiologic uptake). In another case, a patient with well-differentiated adenocarcinoma underwent left hemicolectomy two years before imaging and received chemotherapy continuously for one year. The patient had a history of radiofrequency ablation (RF) of liver metastasis immediately after the last chemotherapy course. After undergoing ^{68}Ga-FAPI-46 PET/CT for response evaluation, the patient underwent liver metastasectomy followed by chemotherapy sessions. Four days later, ^{18}F-FDG PET scan was performed to detect the metastatic lesions. Five liver mass lesions in both liver lobes were observed in both ^{18}F-FDG and FAPI PET scans (Figure 2, left side up and down retrospectively).

In two patients with histopathological confirmation of gastric adenocarcinomas and rising tumor markers (CA=19-9), there were 2 hypermetabolic cervical lymph nodes in the neck region without FAPI uptake (Figures 2, 3). For another patient with a history of papillary thyroid cancer who underwent total thyroidectomy and resection of the right iliac bone, the possibility of initial phases of heterotopic ossification lateral to the resected region of the right sacroiliac bone, could not be ruled out. In this case, both tracers indicated the same involved regions. A patient who had a past diagnosis of GBM located in the right frontotemporal region received surgical removal of the tumor, followed by radiotherapy. The concluding treatment step involved consistent ^{177}Lu-DOTATATE radionuclide therapy. In this case, we performed three different scans for a better assessment of treatment options available in our center. Gallium-68-FAPI- 46 and ^{68}Ga-Pentixafor PET scans exhibited the same uptake in the target region with SUVmax of 1.02 and 4.17, respectively, while ^{68}Ga-DOTATATE PET scan did not indicate any remarkable uptake in the lesion (similar to background). In the known case of Ewing sarcoma (left fibula) who underwent surgical resection and chemotherapy, no abnormal hypermetabolic lesion at the surgical bed (left fibula) was observed. Two hypermetabolic nodules were found in the pulmonary region and paratracheal without FAPI uptake. Discordant uptake of ^{18}F-FDG and FAPI in pulmonary nodule (RUL)

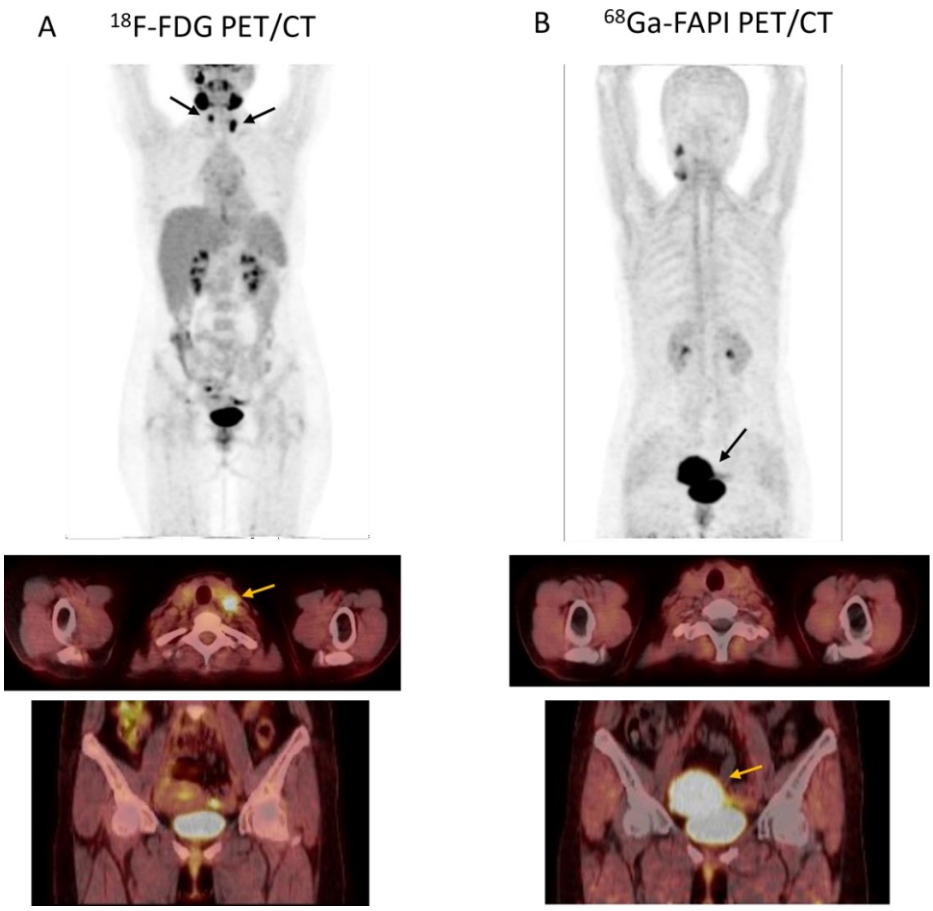

Figure 1. A female patient, aged 45, with metastatic ovarian carcinoma, underwent a ^{68}Ga-FAPI PET/CT scan (on the right) and then, a week later, an ^{18}F-FDG PET/CT scan (on the left). The tracer absorption in the standard liver tissue showed a noticeable variation between the two tracers: SUVmax recorded at 1.22 for ^{68}Ga-FAPI in comparison to a SUVmax of 3.9 for ^{18}F-FDG. When assessing the thyroid nodule and neck lymph node, there was a notably elevated FAPI uptake in contrast to the ^{18}F-FDG uptake.

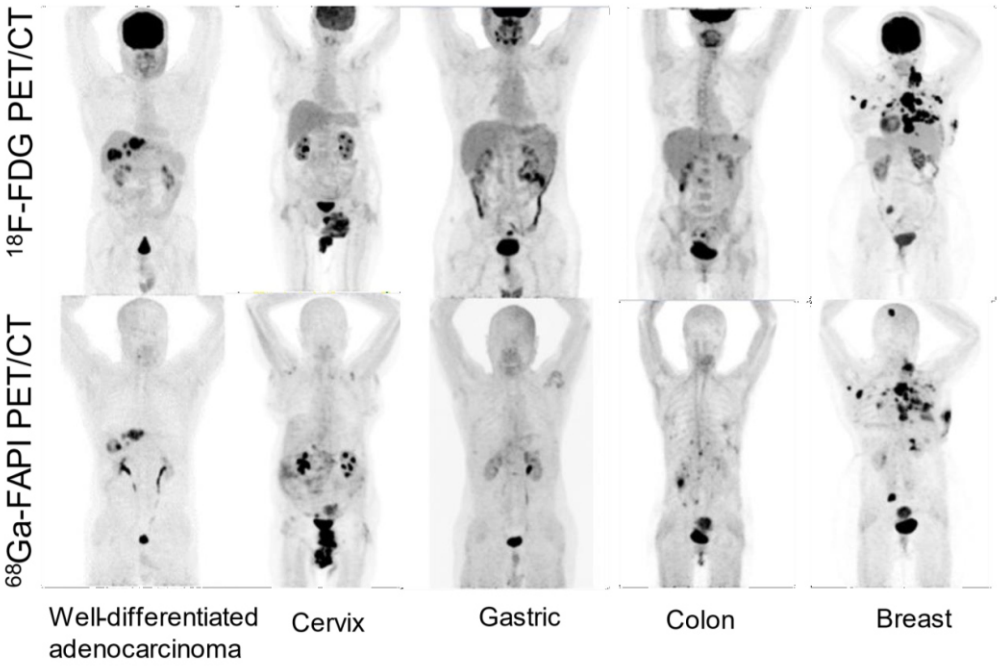

Figure 2. Representative MIP images of ^{68}Ga-FAPI PET/CT and ^{18}F-FDG PET/CT of five different patients with different cancer types.

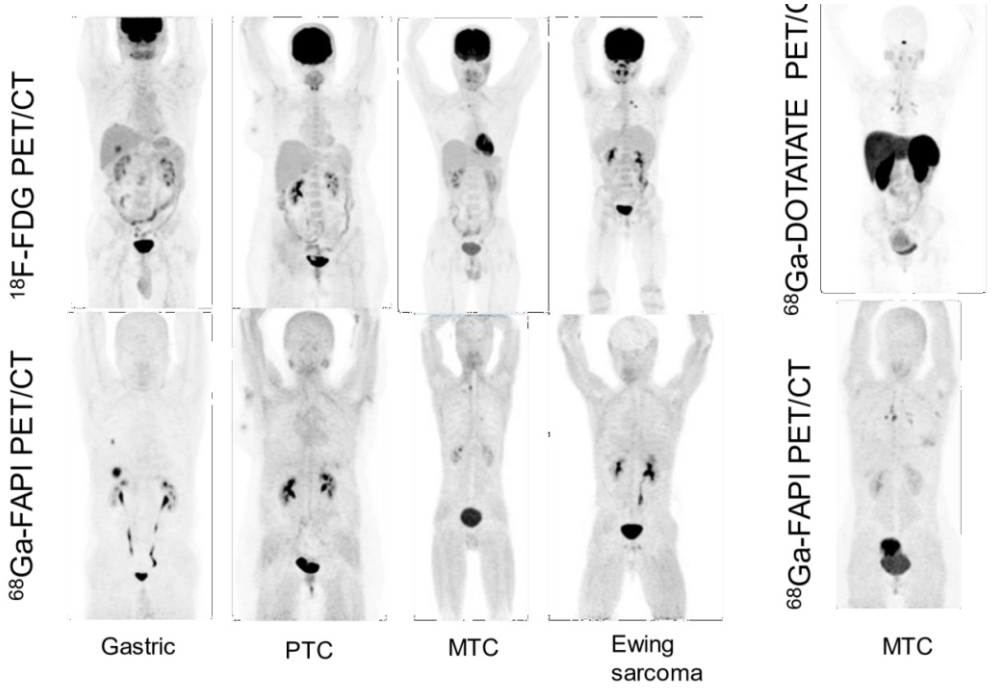

Figure 3. Representative MIP images of ^{18}F-FDG, ^{68}Ga-DOTATATE (first image on top right), and ^{68}Ga-FAPI PET/CT scans with different cancer types.

and paratracheal lymph node required tissue sampling in order to exclude metastatic involvement. Interestingly, two lesions were pathologically diagnosed as malignant and having metastatic involvement. In short, this case showed that if FAPI is negative for recurrence evaluation, imaging using another tracer, such as routine ^{18}F-FDG PET should be performed to distinguish malignant from benign lesions or inflammation (Figure 4).

A known case of colon adenocarcinoma underwent right hemicolectomy and received chemotherapy before ^{18}F-FDG and FAPI imaging. A hypermetabolic peritoneal mass lesion in the right lower quadrant (RLQ) was observed, which is more compatible with peritoneal seeding. In addition, peritoneal nodularities were observed at the surface of the liver, with FAPI uptake compatible with peritoneal seeding. Moreover, two hypermetabolic right renal artery lymph nodes,

linked to patients' history, were more compatible with metastatic involvement. Lung infiltration in the basal left lung observed in ^{18}F-FDG and FAPI scans was more compatible with inflammatory reaction. Three hypermetabolic small mass lesions existed in the right liver lobe (segment 8) that were reflected as metastatic involvement on ^{18}F-FDG PET, while FAPI PET/CT showed no abnormal uptake throughout the liver (Figure 5).

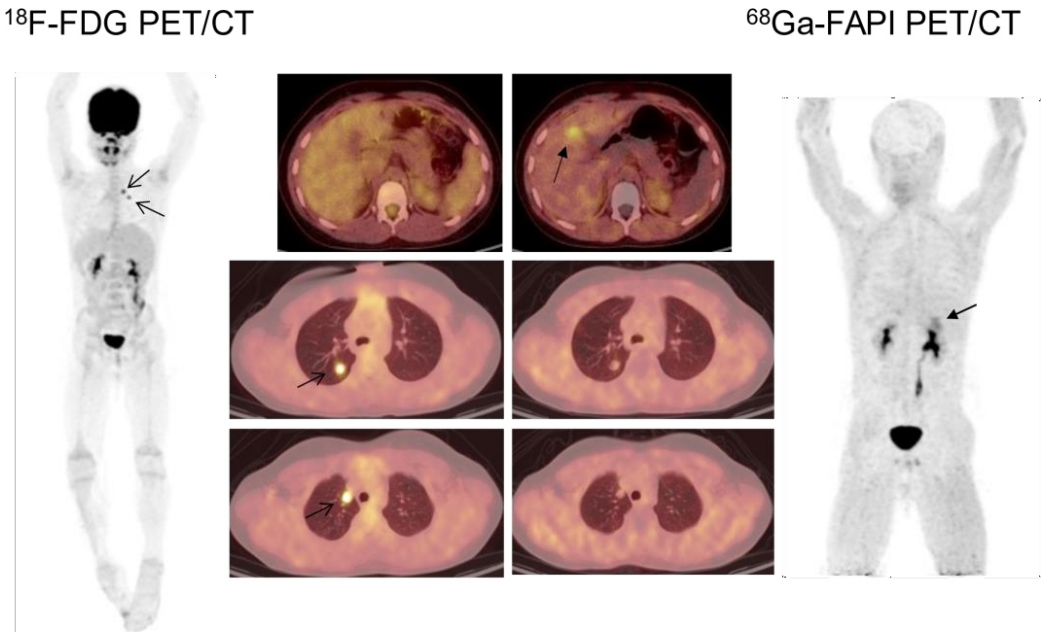

Figure 4. A known case of Ewing sarcoma (involving the left fibula) underwent surgical resection and chemotherapy. No abnormal hypermetabolic lesion existed at the surgical bed (left fibula). Hypermetabolic pulmonary nodule in the RUL with no FAPI uptake was indicated. Hypermetabolic right paratracheal lymph node without FAPI uptake. Discordance between ^{18}F-FDG and FAPI uptake in pulmonary nodule (RUL) and paratracheal lymph node required tissue sampling in order to exclude metastatic involvement. In addition, increased ^{68}Ga-FAPI liver uptake was observed with ^{18}F-FDG non-avidity (upper transverse images).

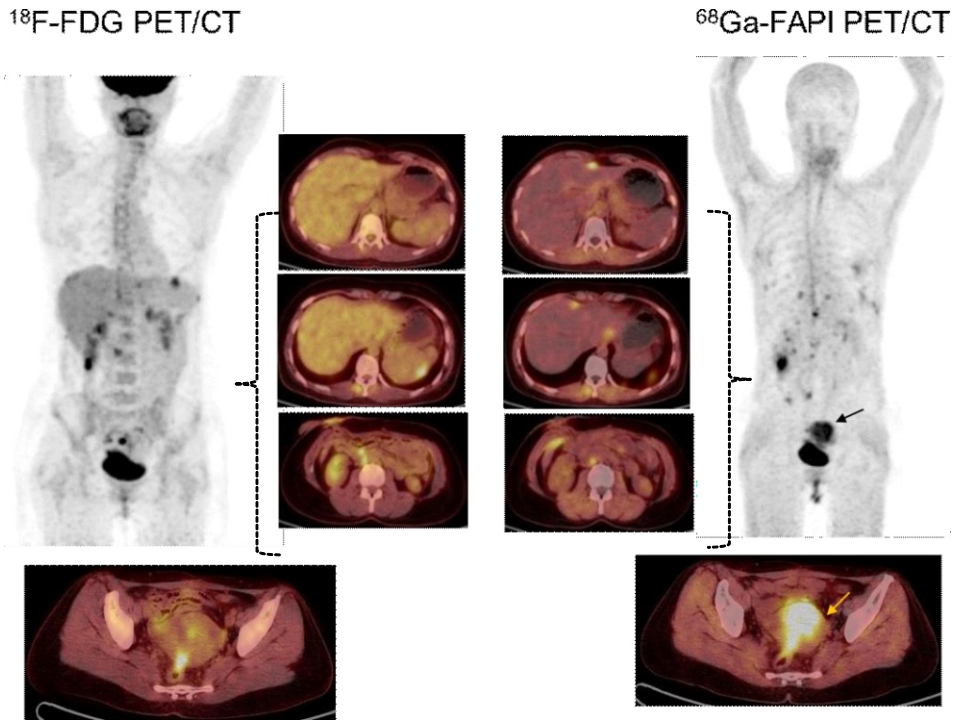

Figure 5. A 41-year-old woman with colon adenocarcinoma underwent hemicolectomy and chemotherapy before ^{18}F-FDG and FAPI scans. Patient results: 1) Hypermetabolic RLQ mass lesion is compatible with peritoneal seeding. Fibroblast activation protein inhibitor uptake is consistent with peritoneal seeding, and liver nodules are peritoneal. 2) Two hypermetabolic right renal artery lymph nodes, which, given the patient's history, suggest metastatic involvement. Left basal lung infiltration with ^{18}F-FDG and FAPI uptake suggests inflammation. 3) Three hypermetabolic small lesions in the right liver lobe (segment 8) suggest metastatic involvement with ^{18}F-FDG non-avidity. Moreover, higher uptake was seen in the uterus in the right lower image in the MIP of the ^{68}Ga-FAPI-46 PET/CT scan.

A patient with breast cancer and two surgical operations underwent one cycle of chemotherapy in combination with ^{177}Lu-Trastuzumab before both FAPI and ^{18}F-FDG imaging. Lymph node involvements in the left axilla (level I), right axilla (level II and III), mediastinum (paratracheal, prevascular, subcarinal), and neck (levels II-V) were visually similar in both PET scans. Left-sided parietal lobe metastasis was clearly found in FAPI PET while the metastatic lesions may have been missed on the ^{18}F-FDG scan due to the high physiologically glucose uptake in the cortex of the brain. The remaining metastases in the lung, sacral bone, and pleural involvement in the right lung was similar in both PET scans (Figure 6).

Two patients with a history of MTC, who underwent peptide receptor radionuclide therapy (PRRT) using one cycle of ^{177}Lu-DOTATATE, were referred for metastatic work-up due to rising calcitonin score (calcitonin scores for patient number 10 and 11 was 2435 and 11173, respectively). In patient #10, paratracheal lymph node metastasis, multiple bilateral non-FAPI avid pulmonary nodules, and a left peri-bronchial lymph node with mild FAPI uptake were found in the FAPI PET scan. Patient #11 showed multiple FAPI-avid lymphadenopathies in the superior mediastinum, paratracheal, pre-carinal, and sub-nodular lesions in both lungs with no ^{18}F-FDG uptake. Gallium-68-FAPI-46 PET/CT scan revealed focal uptake without a corresponding ^{18}F-FDG uptake in a sclerotic lesion at the 9th right rib. Images of the discordant cases were presented in Figure 7. The biopsy test was not available for this patient; therefore, bone metastasis could not be confirmed.

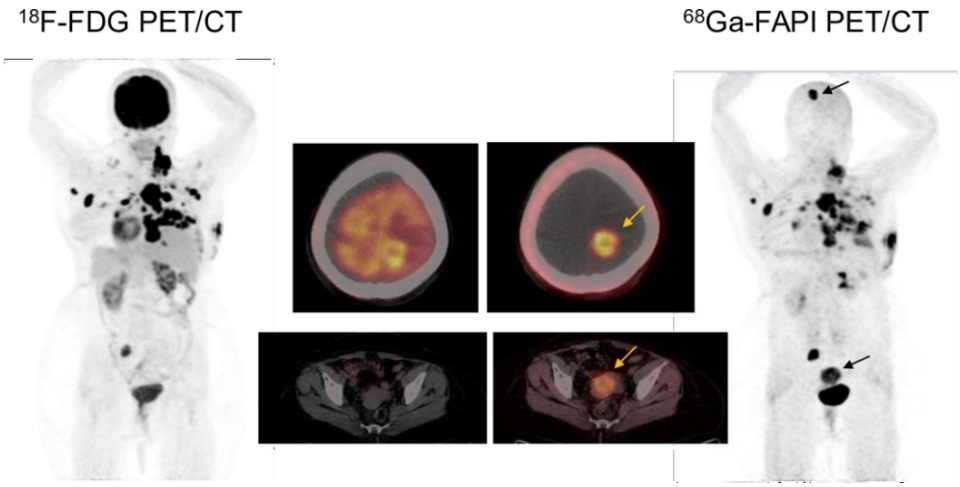

Figure 6. A 48-year-old female with breast cancer. Before FAPI/^{18}F-FDG PET/CT scans, two surgeries and one cycle of chemotherapy in combination with one cycle of ^{177}Lu-Trastuzumab were indicated for this patient. Lymph nodes are involved in the left axilla (level I), right axilla (level II and III), mediastinum (paratracheal, perivascular, subcarinal and in the neck in levels II-V of the right side). Parietal lobe metastasis is clearly indicated in the MIP of FAPI with complicated ^{18}F-FDG uptake due to the high cortex glucose uptake (high background activity). Multiple lung and bone metastasis were seen on images of both tracers.

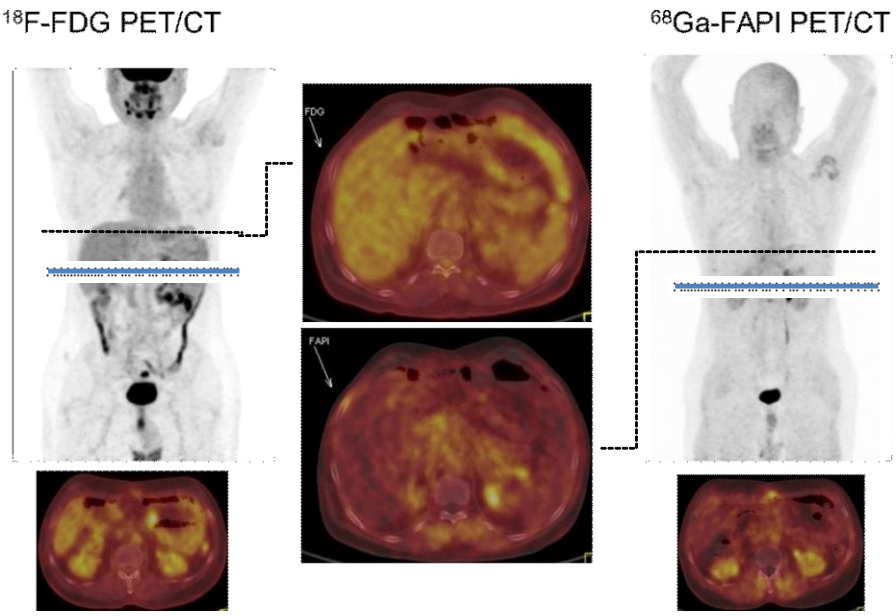

Figure 7. A 65-year-old male with a known case of gastric adenocarcinoma underwent gastrectomy and received CRT. This patient was referred to our center with a rising tumor marker (CA 19-9) and recurrence evaluation. Fibroblast activation protein inhibitor uptake in the focal peritoneal thickening in the midline of the abdomen at a level of L2 (without ^{18}F-FDG hypermetabolism). The mentioned rib lesions showed moderate uptake with ^{18}F-FDG non-avidity.

The false positive result observed in patient #8 in the FAPI PET scan could be justified by post-operative inflammation caused by primary tumor excision about one month before PET studies. Comparative results of ^{18}F-FDG and ^{68}Ga-FAPI-46 PET/CT for recurrence detection are shown in Table 2. A difference in recurrence detection between the ^{18}F-FDG and FAPI scans was observed in 5 out of 11 patients. For detecting cervix and gastric metastases, there wasn't a significant disparity in SUVmax and TBR values between ^{68}Ga-FAPI and ^{18}F-FDG PET/CT. However, in the cases of Ewing sarcoma, MTC, breast, and colon cancer, the SUVmax and TBR figures for ^{68}Ga-FAPI surpassed those of ^{18}F-FDG PET/CT. While the SUVmax values were comparable between the two imaging techniques for spotting liver metastases, the ^{68}Ga-FAPI scan demonstrated a notably higher TBR compared to the ^{18}F-FDG scan, as shown in Table 3. Figures 2 and 3 show examples of maximum intensity projections from ^{18}F-FDG PET/CT and ^{68}Ga-FAPI PET/CT scans of different types of cancer.

Comparison of the uptake of ^{68}Ga-FAPI/^{18}F-FDG, and few cases of ^{68}Ga-Pentixafor/^{68}Ga-DOTATATE in different types of cancer

In the realm of cancer imaging, the application of the ^{68}Ga-FAPI tracer prompts a thorough assessment of lesion detection rates and diagnostic efficacy in comparison to the established oncological radiotracer, ^{18}F-FDG. Chen and colleagues (2021) undertook a comprehensive analysis where ^{68}Ga-FAPI-04 and ^{18}F-FDG PET/CT were subjected to head-to-head evaluation in 75 patients (54 patients during initial assessment and 21 patients for recurrence detection) across a spectrum of 12 distinct tumor types. Their investigation revealed that ^{68}Ga-FAPI-04 exhibited heightened sensitivity compared to ^{18}F-FDG in primary tumors (98.2% vs. 82.1%, P= 0.021), lymph node metastases (86.4% vs. 45.5%, P=0.004), and bone as well as visceral metastases (83.8% vs. 59.5%, P<0.005) [16]. Notably, Qin et al. (2021) reported contrasting findings, indicating that ^{68}Ga-FAPI-04 PET/CT identified a lesser number of positive lymph nodes compared to ^{18}F-FDG PET/CT (48 vs. 100 positive lymph nodes) [28]. Their results inferred that ^{68}Ga-FAPI PET/CT may exhibit enhanced specificity compared to ^{18}F-FDG in distinguishing between reactive lymph nodes and lymph nodes hosting tumor metastasis [29]. Another study focused on ten patients with oral squamous cell carcinoma (OSCC) exhibited similar sensitivity and specificity between ^{68}Ga-FAPI-04 PET/CT and ^{18}F-FDG PET/CT in detecting primary tumors (100% vs. 100%) and cervical lymph node metastases (81.3% vs. 87.5%, P=0.32; 93.3% vs. 81.3%, P=0.16) [30]. However, ^{68}Ga-FAPI-04 PET/CT displayed a higher tumor-to-background ratio (TBR) in comparison to ^{18}F-FDG PET/CT for primary tumor detection (10.90 vs. 4.11) [31]. Komek et al. (2021) provided evidence demonstrating the capabilities of ^{68}Ga- FAPI-04 PET/CT in identifying an increased number of cancer lesions with elevated SUVmax, particularly in primary tumors, lymph nodes, and distant metastases, surpassing the performance of ^{18}F-FDG PET/CT [32, 33]. In yet another study, both ^{18}F-FAPI-42 and ^{18}F-FDG exhibited parallel detection rates (100%) for primary tumors in a cohort of 34 patients. Nonetheless, ^{18}F-FAPI-42 proved less effective in identifying brain lesions compared to contrast-enhanced magnetic resonance imaging (CE-MRI) (56 vs. 34, P<0.005) [34].

Breast cancer

This study showed that the SUVmax of ^{68}Ga-FAPI-46 in breast cancer patients was around 2- fold higher compared to similar studies in the literature. Lymph nodes were observed in the right breast with increased uptake in both ^{18}F-FDG and FAPI scans. The largest lymph node was 34mm in diameter, with SUVmax values of 31.24 and 17.35 for FAPI and ^{18}F-FDG, respectively. Moreover, there was a lesion in the left parietal lobe with 27mm diameter with SUVmax equal to 32.66 and 17.74 in FAPI and ^{18}F-FDG scans, respectively. It should be emphasized that due to the very high absorption of glucose in the brain in ^{18}F-FDG scans, we were not able to find the involved areas and metastases caused by cancers, while the use of FAPI scan bearing minimal brain background, we were able to detect the involved and suspicious areas (Figure 6). Compared to ^{18}F-FDG scans, ^{68}Ga-FAPI scans showed no ties between tracer accumulation and factors like grade, receptor status, or histological variant. While our patient sample was too small to definitively dismiss differences, the results are in sync with immunohistochemical data revealing uniform FAP expression across breast cancer samples, irrespective of the tumor variant [35]. Furthermore, another immunohistochemical investigation pinpointed predominant FAP expression in invasive breast cancers but not in situ ductal carcinomas without microinvasion or typical ductal hyperplasia [36]. The discovery of extra-axillary lymph nodes, which aren't typically suitable for sentinel lymph node biopsy, might guide treatment options in breast cancer cases [37]. For 42% of patients (6 out of 14) who could have been considered for a study evaluating extra-axillary LN metastases, ^{68}Ga-FAPI scans indicated extra-axillary lymph node involvement, compared to the 28% detection rate from the ^{18}F-FDG PET scan [38]. While no direct node-to-node biopsy confirmation of lymph node involvement was presented in these studies, our current findings, combined with consistent accumulation in all confirmed axillary lymph node metastases, advocate for the efficacy of the FAPI PET scan. Its high propensity to detect remote metastases is further bolstered by a case series that juxtaposed ^{68}Ga-FAPI with ^{18}F-FDG PET scans directly [14, 39, 40]. Given the recent introduction of the FAPI radiotracer in our facility, the number of breast cancer scans conducted is limited, hence inhibiting our ability to provide universally applicable diagnostic accuracy values. Earlier research confirmed that ^{68}Ga-FAPI PET/ CT identifies more cancer-related lesions with elevated SUVmax values for primary tumors, including lymph nodes and remote metastases, in contrast to ^{18}F-FDG PET/CT in breast cancer patients [40]. Corroborating this, Komek and team's findings from a 20-patient cohort [33] echo prior FAPI imaging research on breast cancer, underscoring the potential of the ^{68}Ga-FAPI tracer in breast cancer detection.

Papillary thyroid carcinoma (PTC)

Global instances of thyroid cancer are on an upward trajectory, leading to the evolution of novel imaging techniques [41]. To date, there's limited research contrasting the efficacy of FAPI PET/CT with ^{18}F-FDG PET/CT in evaluating differentiated papillary thyroid carcinoma. Beyond ^{18}F-FDG PET/CT,

Table 2. *Comparison of ^{18}F-FDG and ^{68}Ga-FAPI-46 PET/CT scans for recurrence detection.*

Patient No.	Base tumor site	Recurrence site	^{18}F-FDG avidity	^{68}Ga-FAPI-46 avidity	PET/CT result
1	Well differentiated ADC	Liver	Y	Y	*5 liver mass lesion in both liver lobes in the segments of 4,5, 6, 7 showed both ^{18}F-FDG and FAPI uptake and compatible with metastatic involvement. *Progression of disease is noted. (Interval time is 4 days).
2	PTC	Sacroiliac	Y	Y	Possibility of initial phases of heterotopic ossification lateral to the resected region of right sacroiliac bone, cannot be ruled out.
3	Cervix cancer	Peritoneal	N	Y	Comparing with ^{18}F-FDG PET/CT, ^{68}Ga-FAPI PET/CT showed increased activity in the peritoneum and mass lesion in the left side of the pelvic (which is not ^{18}F-FDG avid) more compatible with peritoneal seeding and mesenteric involvement.
4	Gastric ADC	Cervical	Y	N	*Hypermetabolic cervical LN in the right side of the neck (level 2) without FAPI uptake. *FAPI uptake in the focal peritoneal thickening in the mid line of the abdomen at the level of L2 (without hypermetabolism) regarding patient's history more compatible with deposited. For definite diagnosis, tissue sampling is recommended.
5	GBM	Frontotemporal	-	Y	CXCR4 and FAPI avid lesions in the right frontal and right temporal lobes (three mass lesions) more compatible with tumoral recurrence.
6	Gastric ADC	Cardia	Y	N	*Two hepatic metastases are noted in the dome of the liver and in segment VI *No other active lesion is noted in the rest of the body
7	Colon ADC	Peritoneal	Y	N	*Hypermetabolic peritoneal mass lesion in the RLQ more compatible with peritoneal seeding. In addition, there are peritoneal nodularities at the surface of the liver with FAPI uptake more compatible with peritoneal seeding. *Two hypermetabolic right renal artery LNs regarding patient's history more compatible with metastatic involvement. *Lung infiltration in the basal left lung with ^{18}F-FDG and FAPI uptake more compatible with inflammatory reaction. *Three hypermetabolic small mass lesions in the right liver lobe (segment 8) more compatible with metastatic involvement. In FAPI PET/CT the scan showed no abnormal uptake throughout the liver. (No evidence of liver metastatic lesion)
8	Ewing sarcoma	Fibula	Y	N	*Hypermetabolic pulmonary nodule in the RUL without FAPI uptake. *Hypermetabolic right paratracheal LN without FAPI uptake. *Remainder of the study is negative for ^{18}F-FDG and FAPI uptake. *Discordant between ^{18}F-FDG and FAPI uptake in pulmonary nodule (RUL) and paratracheal LN needs tissue sampling in order to exclude metastatic involvement.

(continued)

9	Breast cancer	Breast	Y	Y	Possibility of left breast involvement. Lymph node in the left axilla, right axilla, mediastinum (paratracheal, prevascular, subcarinaland in the neck of the right side. Left-sided parietal bone metastasis. Multiple lung metastases mainly in the right lung. Pleural involvement.
10	MTC	Paratracheal	Y	Y	Right upper paratracheal LN metastasis. Multiple bilateral non-FAPI avid pulmonary nodules. Left peri-bronchial LN with mild FAPI uptake.
11	MTC	Mediastinum	N	Y	Multiple FAPI-avid lymphadenopathies in the superior mediastinum, paratracheal, pre-carinal, and sub-nodular lesions in both lungs with no ^{18}F-FDG uptake.

Table 3. *Comparison of ^{18}F-FDG, ^{68}Ga-FAPI-46, DOTATATE, and Pentixafor SUV in the largest involved lesions.*

Patient	SUVmax (lesion/background) 18F-FDG	SUVmax (lesion/background) FAPI-46	SUVmax (lesion/background) DOTATATE	SUVmax (lesion/background) Pentixafor	TBR
1	5.29/2.63	6.45/1.28	-	-	2.011/5.39
2	12.32/3.99	3.01/2.6	-	-	3.087/1.15
3	4.73/3.61	4.86/1.94	-	-	1.31/2.50
4	9.13/3.8	3.13/1.87	-	-	2.40/1.67
5	-	1.02/0.49	2.45/1.75	4.17/0.23	2.081/1.4/18.13
6	8.50/3.32	24.26/3.32	-	-	2.56/7.37
7	4.59/3.33	7.76/1.44	-	-	1.37/5.38
8	31.24/3.5	17.35/1.2	-	-	8.92/14.45
9	4.52/2.48	14.42/2.9	-	-	1.82/4.97
10	6.46/3.6	5.38/1.52	4.79/10.91	-	1.79/3.53/0.43
11	-	22.44/2.12	5.86/9.42	-	10.58/0.62

it's recognized that various physiological processes in diverse organs can manifest as differential ^{18}F-FDG retentions, especially in the context of infectious/inflammatory activities and other reactive phenomena. Yet, non-specific activities are seldom detected in ^{68}Ga-FAPI PET/CT [14]. Typically, ^{18}F-FDG PET/CT's role in assessing PTC becomes paramount in postoperative scenarios where patients exhibit elevated serum thyroglobulin levels, but present negative outcomes on whole-body radioactive iodine (RAI) scans. However, the merit of employing ^{18}F-FDG PET/CT preoperatively remains a topic of debate [42, 43]. In our study, we focused on the comparison of ^{68}Ga-FAPI-46 and ^{18}F-FDG PET scans in a patient with recurrent thyroid cancer. A 46-year-old woman with a history of PTC underwent total thyroidectomy and resection of the right iliac bone. The possibility of initial phases of heterotopic ossification lateral to the resected region of the right sacroiliac bone cannot be ruled out. There was evidence of right sacroiliac region resection and cement insertion with mild hypermetabolism (SUVmax =5.15), with small zones of possible heterotopic calcification lateral to this region. Based on these results and the features of the tumor, our study showed that ^{68}Ga-FAPI was not inferior to ^{18}F-FDG in a patient

with recurrent papillary thyroid cancer (Figure 3). In addition, ^{68}Ga-FAPI PET can be used as a complementary method with ^{18}F-FDG to detect metastatic foci. According to the literature, $_{18}$F-FDG PET scans bear high sensitivity in less-differentiated thyroid carcinomas compared to well-differentiated ones. However, such a limitation is not observed in ^{68}Ga-FAPI PET scans [42]. This matter calls for a deeper exploration, preferably with a broader patient subset that is more specific. Existing research suggests that ^{68}Ga-FAPI PET imaging boasts enhanced specificity in tumor conditions, given the minimal expression of the fibroblast-activated protein in regular physiological conditions juxtaposed with its heightened expression in cancer-associated fibroblasts amidst tumor cells [16, 44, 45]. The outcomes of this study reinforce the proposition that amalgamating the insights from both PET scans could enhance the precision in pinpointing metastatic locations, especially in intricate scenarios like recurrent papillary thyroid cancer.

Medullary thyroid cancer (MTC)

Preliminary research has indicated a moderate uptake in medullary thyroid cancers, which clouds the significance of FAP imaging [14]. Two patients with a history of MTC who underwent PRRT using one cycle of ^{177}Lu-DOTATATE were referred for a metastatic work- up due to rising calcitonin scores (calcitonin scores for patient #10 and #11 were 2435 and 11173, respectively) (Figure 3). In patient #10, the right upper paratracheal lymph node metastasis, multiple bilateral non-FAPI avid pulmonary nodules, and a left peri-bronchiallymph node with mild FAPI uptake were found. Patient #11 showed multiple FAPI-avid lymphadenopathies in the superior mediastinum, paratracheal, pre-carinal, and subnodular lesions in both lungs with no ^{18}F-FDG uptake.

Sarcomas

Primary lesion detection rates obtained from ^{68}Ga-FAPI-46 and ^{18}F-FDG PET/CT scans were completely different owing to hypermetabolic pulmonary nodules in the pulmonary nodule (RUL) without any FAPI uptake and hypermetabolic right paratracheal lymph nodes without FAPI uptake. A known case of Ewing sarcoma in the left fibula who underwent surgical resection and chemotherapy was referred to our department for pulmonary nodules and a metastatic workup. The discordant uptake of ^{18}F-FDG and FAPI uptake in (RUL) and paratracheal lymph nodes required tissue sampling in order to exclude metastatic involvement. There was a paratracheal lymph node with SUVmax =8.42 (short-axis diameter (SAD)=9mm) and a hypermetabolic pulmonary nodule in the RUL with a diameter of 11mm and SUVmax =6.57 without FAPI uptake. In addition, there is a 5mm pulmonary nodule in the RML without ^{18}F-FDG and FAPI uptake (Figure 4).

Gastric cancer

In the pair of gastric cancer cases we examined, ^{68}Ga-FAPI PET emerged as more adept than ^{18}F-FDG PET in identifying primary lesions and metastases during the initial diagnosis and spotting recurrence in gastric cancer patients. Gallium-68-FAPI PET highlighted an increased number of lesions, or larger ones, with a pronounced tracer absorption. The minimal background uptake by ^{68}Ga-FAPI facilitated the detection of minuscule metastatic gastric cancer lesions in areas such as the peritoneum, abdominal lymph nodes, liver, and bones sites that often prove elusive in an ^{18}F-FDG PET scan (as illustrated in Figure 7). From this perspective, ^{68}Ga-FAPI PET show cased its prowess in delineating both primary and metastatic gastric cancer. Conversely, prior research has documented the relatively modest detection capability of preoperative ^{18}F-FDG PET for primary gastric cancer [46, 47].

Glioblastoma multiform (GBM)

Though glucose-based PET remains the norm for several conditions, amino acid-based PET, such as those using fluoroethyl-L-tyrosine (FET), has demonstrated superiority in glioma research [48]. A combined guideline from prominent associations including the European Association of Nuclear Medicine (EANM), the Society of Nuclear Medicine and Molecular Imaging (SNMMI), the European Association of Neuro-oncology (EANO), and the Working Group for Response Assessment in Neuro-oncology with PET (PETRANO) emphasized the significance of amino acid radiolabeled PET in glioma diagnosis. This guideline also underscored its role in distinguishing genuine progression from treatment-induced alterations like pseudoprogression or radionecrosis [49]. Directly contrasting FET PET with FAP-specific PET in delineating target volume might offer deeper insights into FAP specificity, especially when planning radiation therapy for GBM. However, the ethical concerns surrounding exposing patients to both FET and FAP-specific PET scans, particularly in close succession, are significant, considering the anticipated minimal advantages for the individuals involved. With FAP-specific PET's nascent clinical application in cancer treatment, especially GBM, any threshold setting for individual patients should be overseen by a seasoned nuclear medicine expert [50]. While amino acid and ^{18}F-FDG tracers have been tested for glioma imaging, certain drawbacks like heightened gray matter tracer absorption or diminished uptake in therapy-treated brain regions have been observed [49]. An earlier pilot study employing ^{68}Ga-pentixafor on glioblastoma patients yielded optimistic outcomes, witnessing considerable tumor uptake in 11 of the 13 patients under study [51]. Nevertheless, the limited sample size in that pilot prompted our consideration to evaluate CXCR4 expression levels in glioblastoma cells versus healthy brain tissue in an expanded cohort. The future endeavor aims to gauge the capabilities of ^{68}Ga-Pentixafor and ^{177}Lu-Pentixather as potential diagnostic and therapeutic agents, respectively. In our study, a 55-year-old male with a history of GBM in the right frontotemporal lobes underwent surgical resection, radiotherapy, and ^{177}Lu-DOTATATE for recurrence evaluation. The initial assessment showed that there were three lesions in the cerebral mass of the right frontal and right temporoparietal lobes. These include a lesion in the right frontal lobe with a size of 11×15mm and SUVmax of 4.15 on ^{68}Ga-Pentixafor and SUVmax of 4.28 on ^{68}Ga-FAPI PET images, a lesion in the right frontal lobe (periventricular) with a size of 27×15mm and SUVmax of 1.97 on ^{68}Ga-Pentixafor and SUVmax of 2.68 on ^{68}Ga-FAPI PET images (also spotted on MRI), a lesion in the right temporal lobe with a size of 12× 14mm and SUVmax of 2.23 on 68Ga-Pentixafor and SUVmax

of 1.82 on ^{68}Ga-FAPI PET images. Therefore, CXCR4 and FAPI avid lesions in the right frontal and right temporal lobes (three mass lesions) were more compatible with tumoral recurrence (Figures 8 and 9).

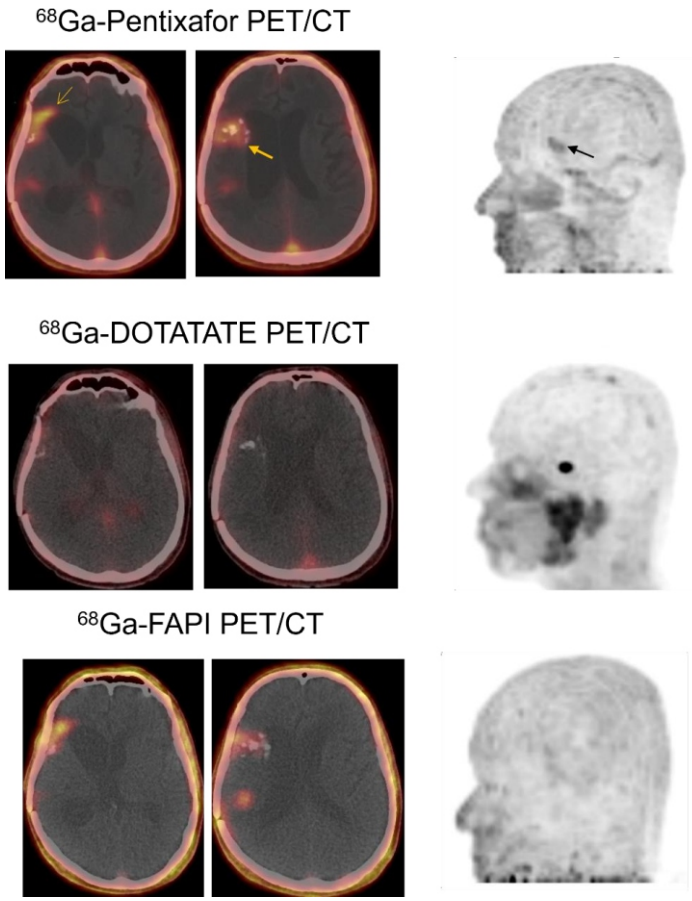

Figure 8. A 55-year-old male with a history of GBM in the right frontotemporal lobes underwent surgical resection and received radiotherapy. After that, he underwent ^{177}Lu-DOTATATE therapy (status: recurrence evaluation). CXCR4 and FAPI avid lesions were observed in the right frontal and right temporal lobes (three mass lesions) more compatible with tumoral recurrence.

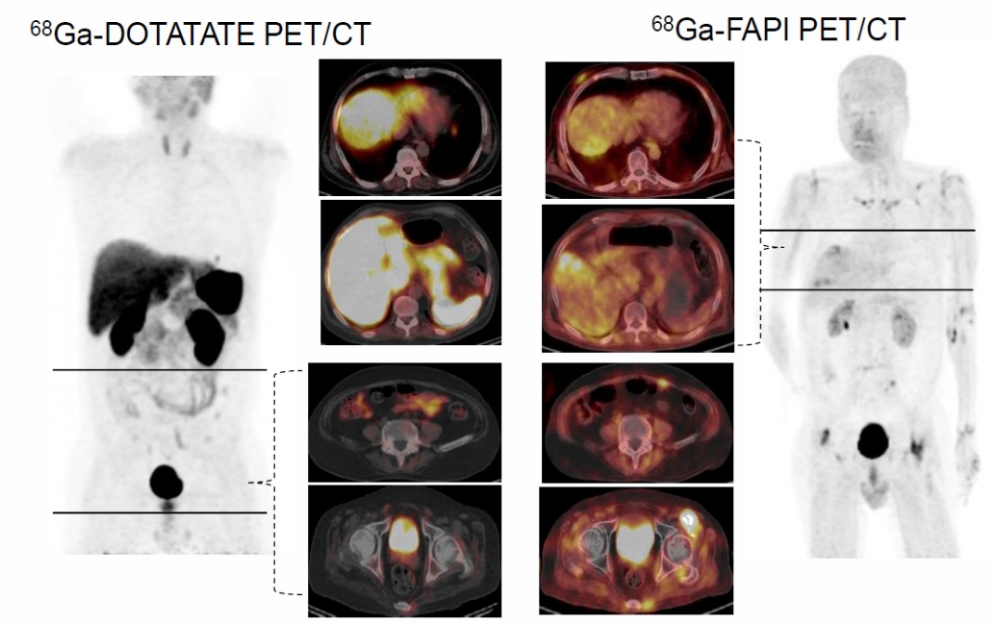

Figure 9. Representative MIP and the involved lesions on ^{68}Ga-DOTATATE (left) and ^{68}Ga-FAPI-46 (right) PET/CT scans of the same patient shown in Figure 8 with a history of GBM in the right frontotemporal lobes who underwent surgical resection and received radiotherapy.

Discussion

The aim of the current investigation was to examine the performance of ^{68}Ga-FAPI-46 compared to the commonly used ^{18}F-FDG PET/CT scan and few cases on ^{68}Ga-DOTATATE/ ^{68}Ga-Pentixafor in the assessment of different types of cancer. Overall, the clinical evaluation showed that ^{68}Ga-FAPI-46 PET/CT offers better lesion visualization and detection compared to other radiotracers. The highest FAPI uptake was found in a hypermetabolic lesion in segment VI of the liver with SUVmax of 24.26 and a size of 39mm (in diameter), while ^{18}F-FDG PET/CT scan showed SUVmax of 8.5. This underscores the potential value of ^{68}Ga-FAPI PET/CT in situations where ^{18}F-FDG PET/CT encounters constraints in regular tissues, like the peritoneal and bowel regions. For instance, due to the subtle uptake of ^{18}F-FDG in low-grade sarcomas, there's a considerable ambiguity between benign and malignant lesions. Even the use of two- time point imaging hasn't mitigated this recognized shortcoming of ^{18}F-FDG PET/CT [52, 53]. Although ^{18}F-FDG PET/CT is frequently used for recurrences in breast cancer, it is not generally recommended for initial staging [54]. However, due to the small number of patients examined with ^{68}Ga-FAPI PET/CT to date, subgroup analysis of histological variants or differentiation grades is not possible. Since the liver is the first target organ for colon cancer metastases, we have reported a significantly lower hepatic background for ^{68}Ga-FAPI-46 (SUVmax=1.02) compared to ^{18}F-FDG with SUVmax of 2.01. This can be beneficial for detecting liver metastases, where in even an intermediate scan in ^{68}Ga-FAPI PET/CT is a reasonable perspective for improving clinical diagnostic performance (Figure 3) [7]. For ovarian cancer, a tumor in the intermediate-intensity group, ^{18}F-FDG may overcome some limitations of conventional imaging but often suffers from heterogeneous uptake into the gut wall due to peristaltic activity [55, 56]. In contrast, ^{68}Ga-FAPI shows very low non-specific intestinal/peritoneal uptake and may be superior for the identification of peritoneal carcinoma, the major clinical challenge in advanced ovarian cancer. A recent analysis indicated that the majority of ^{18}F-FDG PET/CT investigations struggled to distinguish between benign and malignant tumors, attributed to the similar uptake observed in both scenarios [57, 58]. In this regard, a ^{68}Ga-FAPI PET/CT scan would be advantageous for tumor differentiation (e. g., in planning radiotherapy). Distinguishing between residual/recurrent disease and fibrosis after chemoradiotherapy has been reported to pose a diagnostic challenge in ^{18}F-FDG scans [59]. Fluorine-18-FDG PET often performs poorly in neuroendocrine tumors, including medullary thyroid cancer (MTC). This limitation may not be addressed by ^{68}Ga-FAPI since the tumor uptake is also low in FAPI PET images (SUVmax of 6). Comparative semi-quantitative SUVmax in ^{18}F-FDG, ^{68}Ga-DOTATATE, ^{68}Ga-Pentixafor, and ^{68}Ga-FAPI-46 PET/CT for recurrence detection is indicated in Table 4. For colorectal cancer, finding the hypermetabolic peritoneal mass lesions was more complicated on ^{18}F-FDG scans due to the high uptake of the tracer in the peritoneal lesion (Figure 4). In our study, we found that other involvements, such as lung infiltration in the basal left lung with ^{18}F-FDG and FAPI uptake, were more compatible with inflammatory reactions. The tumor-to-background ratio (TBR) in the well-differentiated adenocarcinoma patient (p#1) was 2.01 and 5.39 for ^{18}F-FDG and FAPI PET scans, respectively. These values in a patient with PTC (p#2) were 3.09 for ^{18}F-FDG and 1.15 for FAPI-46. The comparison of ^{18}F-FDG and FAPI TBR in other patients is presented in Table 3. Regarding Table 3, the maximum TBR for ^{18}F-FDG (TBR ^{18}F-FDG= 8.92) and FAPI-46 (TBR FAPI =14.45) was for an Ewing sarcoma patient (p#8). Tumor-to-background ratio in FAPI, DOTATATE, and Pentixafor PET scans were 2.08, 1.40, and 18.13, respectively, in a GBM patient (p#5). In addition, the maximum difference was observed in an MTC patient (p#11) between FAPI and DOTATATE scans with TBR of 10.58 and 0.622, respectively. Therefore, FAPI combined with ^{18}F-FDG imaging may be helpful to find the metastatic involvement. A limited number of cases, expression of heterogeneity, random effects in tissue sampling, and high inter-subject variability appear to be the most appropriate explanations for discrepancies between histological and imaging results. Unlike ^{18}F-FDG studies, which require fasting and rest periods, ^{68}Ga-FAPI PET/CT can be performed 10 minutes to 1 hour after administration [7]. This is an advantage of FAPI over other low molecular weight agents used for prostate cancer imaging, such as PSMA ligands [60]. A retrospective study from a single center [61] evaluated ^{68}Ga-FAPI PET/CT scans in a cohort of 55 patients with uncommon tumors. This included cancer of unknown primary origin (n=10), head and neck cancers (n=13), gastro-intestinal and hepatopancreaticobiliary cancers (n=17), urinary tract cancers (n=4), neuroendocrine tumors (n=4), and various others (n=7). Scans were conducted an hour post-radiotracer injection, utilizing three distinct ^{68}Ga-labeled FAP ligands: FAPI-04, FAPI-46, and FAPI-74. In the semi-quantitative analysis, NET lesions had a higher mean SUVmax than other radiotracers, such as ^{18}F-FDG and ^{68}Ga-DOTATATE. Additionally, multiple case studies have highlighted a notable uptake of ^{68}Ga-FAPI in NET. One instance involved a G2 (Ki-67: 15%-20%) pancreatic NET with liver metastases that underwent a ^{68}Ga-FAPI-04 PET/CT scan following an ^{18}F-FDG PET/CT scan. The results revealed that the ^{68}Ga-FAPI-04 PET/CT detected greater uptake both in the pancreas and in a liver metastasis, which was ^{18}F-FDG-negative, likely due to the reduced background FAPI uptake in the liver [62]. Another case involving a G2 pancreatic NET (Ki- 67: 10%) was assessed with three distinct radiopharmaceuticals: ^{68}Ga-FAPI-04, ^{18}F-FDG, and ^{68}Ga-DOTATATE. The tumor-to-liver ratio was notably higher in the ^{68}Ga-FAPI-04-PET/CT scan compared to the other agents, though ^{68}Ga-DOTATATE was superior in detecting a greater count of minor liver metastases [63]. Our findings harmonize with these earlier studies. Furthermore, Ergül et al. (2022) mentioned that the ^{68}Ga-FAPI-04 PET/CT uptake in a liver NET (Ki- 67: 80%) might surpass that of the ^{18}F-FDG PET/CT. This suggests the potential utility of ^{68}Ga- FAPI-04 PET/CT in NET scenarios where ^{18}F-FDG PET/CT uptake is minimal [64]. To summarize, even though these findings are preliminary, they hint at the FAPI tracer exhibiting a promising biodistribution in NET. Future studies are warranted to further discern the efficacy of ^{68}Ga-FAPI-04 PET/CT in diagnosing and managing NET, especially when there's a pronounced presence of activated fibroblasts [65, 66].

Table 4. *Comparative semi-quantitative of SUVmax in ^{18}F-FDG, ^{68}Ga-DOTATATE, ^{68}Ga-Pentixafor, and ^{68}Ga-FAPI-46 PET/CT for recurrence detection.*

Patient No.	Involved lesion SUVs	Tumor
1	5 hypermetabolic mass lesions involving both liver lobes, including two lesions in segment 6 with a size of 60×32 mm and SUVmax of 14.66, and the other one with a size of 20×23 mm and SUVmax of 11.78. One in segment 5 with a size of 24×37 mm and SUVmax of 15.80. One is in segment 7 with a size of 11×17 mm and SUVmax of 9.38. One in segment 4 with a size of 65×45 mm and SUVmax of 13.56 (all mass lesions showed FAPI uptake as well).	Well- differentiated ADC
2	There is evidence of right sacroiliac region resection and cement insertion with mild hypermetabolism (SUVmax = 5.15), with small zones of possible heterotopic calcification lateral to this region.	PTC
3	Increased FAPI uptake in the peritoneum in the midline of the abdomen and right side of the abdomen, with SUVmax up to 5.03. In addition, there is a mass lesion on the left side of the pelvis with a size of 33×47 mm and SUVmax of 7.31.	Cervix
4	Two hypermetabolic lymph nodes in the right side of the neck, level 2 with SAD= 8 mm and SUVmax of 8.78, and SAD of 6 mm and SUVmax of 9.13 (without FAPI uptake). There is 11×11 mm peritoneal thickening with SUVmax of 5.36 at the level of the L2 vertebra in the mid-abdomen (FAPI uptake without ^{18}F-FDG uptake).	Gastric
5	Three cerebral mass lesions in the right frontal and right temporoparietal lobes, including 11×15 mm with a SUVmax of 4.15 (CXCR4) and SUVmax of 4.28 (FAPI) in the right frontal, 27×15mm in the right frontal lobe (periventricular), which is indicated in MRI, with SUVmax of 1.97 (CXCR4) and SUVmax of 2.68 (FAPI), and the third lesion with a size of 12×14 mm in the right temporal lobe and SUVmax 2.23 (CXCR4) and 1.82 (FAPI).	GBM
6	The liver shows a large hypoattenuating hypermetabolic lesion in segment VI with 39 mm diameter and SUVmax=8.5 on ^{18}F-FDG and 24.26 on FAPI scan. There is a small lesion in the dome of the right hepatic lobe around 16 mm with SUVmax=4.19 on ^{18}F-FDG and 12.45 on the FAPI scan.	Gastric
7	The RLQ at L4 level has 14-15 mm of hypermetabolic peritoneal mass with SUVmax of 10.35. There are two hypermetabolic lymph nodes at the level of the right renal kidney, with SAD=11mm and SUVmax=5.65, and SAD = 12mm and SUVmax=4.90. The spleen was normal in size and revealed a focal hypermetabolic lesion with SUVmax of 6.20. The liver is normal in size and texture, with three hypermetabolic small mass lesions in the right liver lobe, with SUVmax up to 4.18 in segment 8.	Colon
8	Paratracheal LN with SAD=9mm and SUVmax=8.42.There are no abnormally hypermetabolic lymph nodes in the axillae. There is a hypermetabolic pulmonary nodule in the RUL with a diameter of 11 mm and SUVmax 6.57 which showed no FAPI uptake. In addition, there is a 5-mm pulmonary nodule in the RML without ^{18}F-FDG and FAPI uptake.	Ewing sarcoma
9	Lymph nodes on the right side with increased uptake in both ^{18}F-FDG and FAPI scans. The largest lymph node is 34mm in diameter, with SUVmax=31.24 (^{18}F-FDG) and 17.35 (FAPI). There is a lesion in the left parietal lobe with a diameter of 27 mm, and SUVmax of 32.66 of ^{18}F-FDG and 17.74 for FAPI.	Breast
10	A left peri-bronchial lymph node with mild FAPI uptake (SUVmax =3.30). There are multiple pulmonary nodules in both lungs with no FAPI uptake; the largest one is 10.6 mm in the RML (SUVmax =0.87).	MTC
11	A 1 cm lymph node in the superior mediastinum (SUVmax =3.31 on the left). Multiple lymph nodes were noted in the paratracheal, pre-carinal, sub-carinal, and bilateral hilar with high FAPI uptake (SUVmax up to 9.68).	MTC

In conclusion, the use of ^{68}Ga-labeled FAPI variants has shown encouraging results in a variety of cancers. Since ^{18}F-FDG is the preeminent tracer in clinical oncology at the moment, it is necessary to conduct well-designed clinical trials with sizable patient populations to define the role of this diagnostic radiotracer. Fibrosis, arthritis, atherosclerosis, and autoimmune diseases have all been linked to high levels of FAP expression, in addition to CAF. Fibroblast activation protein inhibitor uptake in non-malignant diseases necessitates careful diagnosis. Overall, we found that ^{68}Ga-FAPI PET/CT has diagnostic performance that is comparable with or even superior to that of ^{18}F-FDG PET/CT for a number of cancer types, especially those that typically shows low to moderate ^{18}F-FDG uptake. Moreover, ^{68}Ga-FAPI results in greater TBR compared to ^{18}F-FDG because of the lower background uptake in normal organs. Fasting is not necessary for ^{68}Ga-FAPI PET/CT, making it an advantage over ^{18}F-FDG PET/CT in the sense that image acquisition can begin soon after injection (10-60min p.i.). Compared to ^{18}F-FDG, ^{68}Ga-Pentixafor, and ^{68}Ga-DOTATATE radiotracers, ^{68}Ga-FAPI-46 PET images led to higher detection rates for most metastases and better patient classification. Future research into FAP-targeted radionuclide therapy should look into chemically modifying tracers to improve their pharmacokinetic properties.

The authors declare that they have no conflicts of interest.

Bibliography

1. Roma-Rodrigues C, Mendes R, Baptista PV, Fernandes AR. Targeting Tumor Microenvironment for Cancer Therapy. *Int J Mol Sci* 2019; 20(4): 840.
2. von Ahrens D, Bhagat TD, Nagrath D et al. The role of stromal cancer-associated fibroblasts in pancreatic cancer. *J Hematol Oncol* 2017; 10(1): 76.
3. Shiga K, Hara M, Nagasaki T et al. Cancer-associated fibroblasts: their characteristics and their roles in tumor growth. *Cancers* 2015; 7(4): 2443-58.
4. Moreno-Ruiz P, Corvigno S, Te Grootenhuis NC et al. Stromal FAP is an independent poor prognosis marker in non-small cell lung adenocarcinoma and associated with p53 mutation. *Lung Cancer* 2021; 155: 10-9.
5. Zou B, Liu X, Zhang B et al. The Expression of FAP in Hepatocellular Carcinoma Cells is Induced by Hypoxia and Correlates with Poor Clinical Outcomes. *J Cancer* 2018; 9(18): 3278-86.
6. Wikberg ML, Edin S, Lundberg IV et al. High intratumoral expression of fibroblast activation protein (FAP) in colon cancer is associated with poorer patient prognosis. *Tumour Biol* 2013; 34(2): 1013-20.
7. Giesel FL, Kratochwil C, Lindner T et al. ^{68}Ga-FAPI PET/CT: Biodistribution and Preliminary Dosimetry Estimate of 2 DOTA-Containing FAP-Targeting Agents in Patients with Various Cancers. *J Nucl Med* 2019; 60(3): 386-92.
8. Lindner T, Loktev A, Altmann A et al. Development of Quinoline-Based Theranostic Ligands for the Targeting of Fibroblast Activation Protein. *J Nucl Med* 2018; 59(9): 1415-22.
9. Hathi DK, Jones EF. ^{68}Ga FAPI PET/CT: Tracer Uptake in 28 Different Kinds of Cancer. *Radiol Imaging Cancer* 2019; 1(1): e194003.
10. Loktev A, Lindner T, Mier W et al. A Tumor-Imaging Method Targeting Cancer-Associated Fibroblasts. *J Nucl Med* 2018; 59(9): 1423-9.
11. Loktev A, Lindner T, Burger EM et al. Development of Fibroblast Activation Protein-Targeted Radiotracers with Improved Tumor Retention. *J Nucl Med* 2019; 60(10): 1421-9.
12. Ferdinandus J, Kessler L, Hirmas N et al. Equivalent tumor detection for early and late FAPI-46 PET acquisition. *Eur J Nucl Med Mol Imaging* 2021; 48(10): 3221-7.
13. Chen H, Zhao L, Ruan D et al. Usefulness of ^{68}Ga-DOTA-FAPI-04 PET/CT in patients presenting with inconclusive ^{18}F-FDG PET/CT findings. *Eur J Nucl Med Mol Imaging* 2021; 48(1): 73-86.
14. Kratochwil C, Flechsig P, Lindner T et al. ^{68}Ga-FAPI PET/CT: Tracer Uptake in 28 Different Kinds of Cancer. *J Nucl Med* 2019; 60(6): 801-5.
15. Pang Y, Zhao L, Luo Z et al. Comparison of ^{68}Ga-FAPI and ^{18}F-FDG Uptake in Gastric, Duodenal, and Colorectal Cancers. *Radiology* 2021; 298(2): 393-402.
16. Chen H, Pang Y, Wu J et al. Comparison of ^{68}Ga-DOTA-FAPI-04 and ^{18}F-FDG PET/CT for the diagnosis of primary and metastatic lesions in patients with various types of cancer. *Eur J Nucl Med Mol Imaging* 2020; 47(8): 1820-32.
17. Wei Y, Cheng K, Fu Z et al. ^{18}F-AlF-NOTA-FAPI-04 PET/CT uptake in metastatic lesions on PET/CT imaging might distinguish different pathological types of lung cancer. *Eur J Nucl Med Mol Imaging* 2022; 49(5): 1671-81.
18. Zhao L, Chen S, Lin L et al. ^{68}Ga-DOTA-FAPI-04 improves tumor staging and monitors early response to chemoradiotherapy in a patient with esophageal cancer. *Eur J Nucl Med Mol Imaging* 2020; 47(13): 3188-9.
19. Hofheinz RD, al-Batran SE, Hartmann F et al. Stromal antigen targeting by a humanised monoclonal antibody: an early phase II trial of sibrotuzumab in patients with metastatic colorectal cancer. *Onkologie* 2003; 26(1): 44-8.
20. Bozkurt MF, Virgolini I, Balogova S et al. Guideline for PET/CT imaging of neuroendocrine neoplasms with ^{68}Ga-DOTA-conjugated somatostatin receptor targeting peptides and ^{18}F-DOPA. *Eur J Nucl Med Mol Imaging* 2017; 44(9): 1588-601.
21. Treglia G, Sadeghi R, Giovinazzo F et al. PET with Different Radiopharmaceuticals in Neuroendocrine Neoplasms: An Umbrella Review of Published Meta-Analyses. *Cancers (Basel)* 2021; 13(20): 5172.
22. Sundin A, Arnold R, Baudin E et al. ENETS Consensus Guidelines for the Standards of Care in Neuroendocrine Tumors: Radiological, Nuclear Medicine & Hybrid Imaging. *Neuroendocrinology* 2017; 105(3): 212-44.
23. Bian XW, Yang SX, Chen JH et al. Preferential expression of chemokine receptor CXCR4 by highly malignant human gliomas and its association with poor patient survival. *Neurosurgery* 2007; 61(3): 570-8; discussion 8-9.
24. Lange F, Kaemmerer D, Behnke-Mursch J et al. Differential somatos--tatin, CXCR4 chemokine and endothelin A receptor expression in WHO grade I-IV astrocytic brain tumors. *J Cancer Res Clin Oncol* 2018; 144(7): 1227-37.
25. Ma X, Shang F, Zhu W, Lin Q. CXCR4 expression varies significantly among different subtypes of glioblastoma multiforme (GBM) and its low expression or hypermethylation might predict favorable overall survival. *Expert Rev Neurother* 2017; 17(9): 941-6.
26. Yordanova A, Biersack HJ, Ahmadzadehfar H. Advances in Molecular Imaging and Radionuclide Therapy of Neuroendocrine Tumors. *J Clin Med* 2020; 9(11): 3679.
27. Lapa C, Hänscheid H, Kircher M et al. Feasibility of CXCR4-Directed Radioligand Therapy in Advanced Diffuse Large B-Cell Lymphoma. *J Nucl Med* 2019; 60(1): 60-4.
28. Qin C, Liu F, Huang J et al. A head-to-head comparison of ^{68}Ga-DOTA-FAPI-04 and ^{18}F-FDG PET/MR in patients with nasopharyngeal carcinoma: a prospective study. *Eur J Nucl Med Mol Imaging* 2021; 48(10): 3228-37.
29. Shang Q, Zhao L, Pang Y et al. ^{68}Ga-FAPI PET/CT Distinguishes the Reactive Lymph Nodes From Tumor Metastatic Lymph Nodes in a Patient With Nasopharyngeal Carcinoma. *Clin Nucl Med* 2022; 47(4): 367-8.
30. Linz C, Brands RC, Kertels O et al. Targeting fibroblast activation protein in newly diagnosed squamous cell carcinoma of the oral cavity - initial experience and comparison to ^{18}F-FDG PET/CT and MRI. *Eur J Nucl Med Mol Imaging* 2021; 48(12): 3951-60.
31. Schirbel A, Lindner T, Meyer T et al. Improved cancer detection in Waldeyer's tonsillar ring by ^{68}Ga-FAPI PET/CT imaging. *Eur J Nucl Med Mol Imaging* 2021; 48(4): 1178-87.
32. Elboga U, Sahin E, Kus T et al. Superiority of ^{68}Ga-FAPI PET/CT scan in detecting additional lesions compared to ^{18}F-FDG PET/CT scan in breast cancer. *Ann Nucl Med* 2021; 35(12): 1321-31.
33. Kömek H, Can C, Güzel Y et al. ^{68}Ga-FAPI-04 PET/CT, a new step in breast cancer imaging: a comparative pilot study with the ^{18}F-FDG PET/CT. *Ann Nucl Med* 2021; 35(6): 744-52.
34. Li Y, Lin X, Li Y et al. Clinical Utility of F-18 Labeled Fibroblast Activation Protein Inhibitor (FAPI) for Primary Staging in Lung Adenocarcinoma: a Prospective Study. *Mol Imaging Biol* 2022; 24(2): 309-20.
35. Tchou J, Zhang PJ, Bi Y et al. Fibroblast activation protein expression by stromal cells and tumor-associated macrophages in human breast

cancer. Hum Pathol 2013; 44(11): 2549-57.
36. Hua X, Yu L, Huang X et al. Expression and role of fibroblast activation protein-alpha in microinvasive breast carcinoma. *Diagn Pathol* 2011; 6: 111.
37. Kirchner J, Martin O, Umutlu L et al. Impact of ^{18}F-FDG PET/MR on therapeutic management in high risk primary breast cancer patients - A prospective evaluation of staging algorithms. *Eur J Radiol* 2020; 128: 108975.
38. Bagheri H, Mahdavi SR, Geramifar P et al. An Update on the Role of mpMRI and ^{68}Ga-PSMA PET Imaging in Primary and Recurrent Prostate Cancer. *Clin Genitourin Cancer* 2024; 22(3): 102076.
39. Pang Y, Zhao L, Chen H. ^{68}Ga-FAPI Outperforms ^{18}F-FDG PET/CT in Identifying Bone Metastasis and Peritoneal Carcinomatosis in a Patient With Metastatic Breast Cancer. *Clin Nucl Med* 2020; 45(11): 913-5.
40. Ballal S, Yadav MP, Moon ES et al. Biodistribution, pharmacokinetics, dosimetry of ^{68}Ga-DOTA.SA.FAPi, and the head-to-head comparison with ^{18}F-FDG PET/CT in patients with various cancers. *Eur J Nucl Med Mol Imaging* 2021; 48(6): 1915-31.
41. Davies L, Hoang JK. Thyroid cancer in the USA: current trends and outstanding questions. *Lancet Diabetes Endocrinol* 2021; 9(1): 11-2.
42. Piccardo A, Puntoni M, Bertagna F et al. ^{18}F-FDG uptake as a prognostic variable in primary differentiated thyroid cancer incidentally detected by PET/CT: a multicentre study. *Eur J Nucl Med Mol Imaging* 2014; 41(8): 1482-91.
43. Kim SK, So Y, Chung HW et al. Analysis of predictability of F-18 fluorodeoxyglucose-PET/CT in the recurrence of papillary thyroid carcinoma. *Cancer Med* 2016; 5(10): 2756-62.
44. Taveira M. Comparison of ^{68}Ga-FAPI versus ^{18}F-FDG PET/CT for Initial Cancer Staging. R*adiol Imaging Cancer* 2021; 3(2): e219007.
45. Ou L, Wu J, Yang F, Zhang C. Comparison of ^{68}Ga-FAPI and ^{18}F-FDG PET/CT inmetastasis of thyroid papillary carcinoma. *Hell J Nucl Med* 2021; 24(1): 100-1.
46. Liu R, Li H, Liu L et al. Fibroblast activation protein: A potential therapeutic target in cancer. *Cancer Biol Ther* 2012; 13(3): 123-9.
47. Röhrich M, Loktev A, Wefers AK et al. IDH-wildtype glioblastomas and grade III/IV IDH-mutant gliomas show elevated tracer uptake in fibroblast activation protein-specific PET/CT. *Eur J Nucl Med Mol Imaging* 2019; 46(12): 2569-80.
48. Albert NL, Weller M, Suchorska B et al. Response Assessment in Neuro-Oncology working group and European Association for Neuro-Oncology recommendations for the clinical use of PET imaging in gliomas. *Neuro Oncol* 2016; 18(9): 1199-208.
49. Law I, Albert NL, Arbizu J et al. Joint EANM/EANO/RANO practice guidelines/SNMMI procedure standards for imaging of gliomas using PET with radiolabelled amino acids and ^{18}F-FDG: version 1.0. *Eur J Nucl Med Mol Imaging* 2019; 46(3): 540-57.
50. Piroth MD, Pinkawa M, Holy R et al. Integrated boost IMRT with FET-PET-adapted local dose escalation in glioblastomas. Results of a prospective phase II study. *Strahlenther Onkol* 2012; 188(4): 334-9.
51. Lapa C, Lückerath K, Kleinlein I et al. ^{68}Ga-Pentixafor-PET/CT for Imaging of Chemokine Receptor 4 Expression in Glioblastoma. *Theranostics* 2016; 6(3): 428-34.
52. Parghane RV, Basu S. Dual-time point ^{18}F-FDG-PET and PET/CT for Differentiating Benign From Malignant Musculoskeletal Lesions: Opportunities and Limitations. *Semin Nucl Med* 2017; 47(4): 373-91.
53. Tagliabue L, Del Sole A. Appropriate use of positron emission tomography with ^{18}F-fluorodeoxyglucose for staging of oncology patients. *Eur J Intern Med* 2014; 25(1): 6-11.
54. Caresia Aroztegui AP, García Vicente AM, Alvarez Ruiz S et al. ^{18}F-FDG PET/CT in breast cancer: Evidence-based recommendations in initial staging. *Tumour Biol* 2017; 39(10): 1010428317728285.
55. Marzola MC, Chondrogiannis S, Rubello D. Fludeoxyglucose ^{18}F- PET/CT Assessment of Ovarian Cancer. *PET Clin* 2018; 13(2): 179-202.
56. Kitajima K, Murakami K, Sakamoto S et al. Present and future of FDG-PET/CT in ovarian cancer. Ann Nucl Med 2011; 25(3): 155-64.
57. Bertagna F, Nicolai P, Maroldi R et al. Diagnostic role of ^{18}F-FDG-PET or PET/CT in salivary gland tumors: A systematic review. *Rev Esp Med Nucl Imagen Mol* 2015; 34(5): 295-302.
58. Plaxton NA, Brandon DC, Corey AS et al. Characteristics and Limitations of FDG PET/CT for Imaging of Squamous Cell Carcinoma of the Head and Neck: A Comprehensive Review of Anatomy, Metastatic Pathways, and Image Findings. *Am J Roentgenol* 2015; 205(5): W519-31.
59. Lai V, Khong PL. Updates on MR imaging and ^{18}F-FDG PET/CT imaging in nasopharyngeal carcinoma. *Oral Oncol* 2014; 50(6): 539-48.
60. Afshar-Oromieh A, Hetzheim H, Kübler W et al. Radiation dosimetry of ^{68}Ga-PSMA-11 (HBED-CC) and preliminary evaluation of optimal imaging timing. *Eur J Nucl Med Mol Imaging* 2016; 43(9): 1611-20.
61. Dendl K, Finck R, Giesel FL et al. FAP imaging in rare cancer entities-first clinical experience in a broad spectrum of malignancies. *Eur J Nucl Med Mol Imaging* 2022; 49(2): 721-31.
62. Wang H, Du Z, Huang Q et al. The superiority of ^{68}Ga-FAPI-04 over ^{18}F-FDG in a case of neuroendocrine tumour with hepatic metastasis. *Eur J Nucl Med Mol Imaging* 2021; 48(9): 3005-6.
63. Cheng Z, Zou S, Cheng S et al. Comparison of ^{18}F-FDG, ^{68}Ga-FAPI, and ^{68}Ga-DOTATATE PET/CT in a Patient With Pancreatic Neuroendocrine Tumor. *Clin Nucl Med* 2021; 46(9): 764-5.
64. Ergül N, Yılmaz B, Cin M, Çermik TF. ^{68}Ga-DOTA-FAPI-04 PET/CT in Neuroendocrine Carcinoma of the Liver With Elevated AFP Level: Comparison With ^{18}F-FDG PET/CT. *Clin Nucl Med* 2022; 47(1): e29-e31.
65. Kömek H, Gündoğan C, Can C. ^{68}Ga-FAPI PET/CT Versus ^{68}Ga-DOTATATE PET/CT in the Evaluation of a Patient With Neuroendocrine Tumor. *Clin Nucl Med* 2021; 46(5): e290-e2.
66. Dadgar H, Norouzbeigi N, Jafari E et al. Exploring the efficacy of FAPI PET/CT in the diagnosis and treatment management of colorectal cancer: a comprehensive literature review and initial experience. *Clin Transl Imaging* 2024; 12(1): 1-18.